# Numerical Evaluation of Slope Stability based on Temporal Variation of Hydraulic Conductivity

*Alinda* Gupta[1], *Md Azijul* Islam[2], and *Md Jobair Bin* Alam[3*]

[1]Graduate Research Assistant, Department of Civil Engineering, The University of Texas at Arlington, Texas, USA
[2]Assistant Professor of Instruction, Department of Civil Engineering, The University of Texas at Arlington, Texas, USA
[3]Assistant Professor, Department of Civil Engineering, Prairie View A&M University, Texas, USA

**Abstract.** Slope failure is a common phenomenon all over the world on both man-made and natural slopes. Prolonged rainfall is one of the climatic factors which is largely responsible for slope failure. During heavy and prolonged rainfall, a part of the rainwater infiltrates through the soil and seeps into the slope. The infiltrated water lowers the matric suction and increases the porewater pressure. Eventually, the generated porewater pressure decreases the strength of the soil which results in slope failures. To evaluate the effect of rainwater seepage on slope stability, it is necessary to investigate the hydraulic conductivity of the slope soil. The objective of this study is to evaluate the effect of hydraulic conductivity on slope failure mechanisms. A finite element analysis of slope stability was conducted using Geo-Studio software. A numerical model was developed and calibrated with field monitoring data. The field monitoring data included the observation of hydraulic conductivity using a Guelph Permeameter. Afterward, the temporal variation of rainfall and hydraulic conductivity was incorporated into the SEEP/W program and the consequent changes in slope stability were evaluated in SLOPE/W. From the numerical analysis, with the identical strength parameters of the soil, different factors of safety were observed when the slope sections retain different hydraulic properties. Based on the numerical analysis, it was observed that hydraulic conductivity greater than $4\times10^{-6}$ cm/s leads to slope failure. Periodic monitoring of hydraulic conductivity in the field may provide deep insight into rainfall-induced slope failures.

**Keywords:** Slope Stability, Hydraulic conductivity, Guelph Permeameter, Unsaturated Soil

## 1 Introduction

Slope failures and landslides are major disasters all over the world and cause substantial economic loss and fatalities [1]. These failures occur in both natural and man-made slopes. The problem is prominent in areas where highway embankments and other man-made slopes are constructed on high plastic clay. High plastic clay typically has sufficient strength to hold the slope in place in a dry condition. However, this type of soil is prone to cyclic swelling and shrinkage under weather loadings such as precipitation and evapotranspiration [2]. In Texas, most of the highway slopes are built on expansive soil containing the most swelling potential mineral: Montmorillonite, which is susceptible to cyclic weather loadings. The Texas Department of Transportation (TxDOT) spends a million dollars to repair the failed slopes and for annual maintenance along the state roads and highways. Moreover, it impedes regular mobility and causes significant time loss for commuters.

The failure mechanism of slope built with expansive soil due to precipitation is a complex process that requires an understanding of unsaturated soil mechanics. The soil hydraulic properties concerning matric suction and moisture content follow a nonlinear relationship. The rapid changes in pore-water pressure and moisture variation have a significant effect on the soil strength, consequently the stability of the slopes. The soil tends to soften over time, reducing the effective shear strength and reducing the factor of safety [3]. During the dry seasons, the expansive soil cracks, and lose its integrity. Moreover, shrinkage cracks that develop on slopes act as a conduit for rainfall infiltration, providing a potential flow path for the water to seep through. The combination of the prolonged rainfall and the cyclic swelling and shrinking causes the highway slope more prone to failure.

The presence of desiccation cracks can significantly affect soil hydro-mechanical behavior, including volume change in clay, slaking, permeability, residual shear, and tensile strength [4]. Moreover, high plasticity clayey soil loses its shear strength properties, mainly cohesion intercept c′, after undergoing cyclic wetting and drying periods [5]. During any rainfall event, the rainwater seeps through the crack surface quickly and saturates the soil, reduces soil shear strength by decreasing its matric potential, and decreases the effective stress by increasing pore water pressure. Consequently, the resisting forces of the slope that hold

* Corresponding author: mdalam@pvamu.edu

the soil in place decrease, and the driving forces increase, and eventually, this results in rainfall-induced slope failures [6].

Several researchers performed field investigations, laboratory flume tests, and numerical simulations to investigate slope failure mechanisms and identify the criteria for initiating slope failure [7, 8]. The conventional criteria include the development of excessive strain, shifting of the ground, rising water level, advancing wetting front, and cracking or loosening of the slope surface. When any of those above-mentioned criteria changes abruptly, it is generally considered an imminent slope failure, and the corresponding rainfall event is called critical rainfall. Those slope failure indicators can be monitored by field instrumentation such as slope movement monitoring through tilt sensors, inclinometer, and extensometer; soil moisture variation through dielectric moisture sensors and tensiometer; groundwater level through piezometer. However, extensive instrumentation all over the slope of a highway embankment is practically infeasible because of the high costs of instrumentation and subsequent monitoring for a long time.

Another approach to determining the failure criteria is to perform numerical studies by incorporating the precipitation effect. Researchers conducted coupled and uncoupled seepage and slope stability analyses to determine the time required for slope failure for different cases [9]. The main conceptual difference between saturated and unsaturated soil shear strength is the additional shear strength induced by soil matric suction. Finite element method (FEM) based computer programs such as SEEP/W, PLAXIS 2D PlaxFlow, SVFLUX, Geo5, etc. are commonly being used for seepage analyses. Slope stability analyses can be executed using Limit Equilibrium (LE), FEM, and probabilistic method [10]. In recent years, the development of more advanced modules in GeoStudio that includes transient seepage and deformation analysis in which soil variables can be incorporated provides the option for rigorous analyses in rainfall-induced slope failure. Moreover, the uncouple analyses (seepage and slope, & deformation and slope) become popular for transient seepage analyses.

A method for slope-failure monitoring can be based on the observation of the Hydraulic properties of soil and its changes over time at shallow depths. Several studies show the numerical modeling and analysis of physical parameters to develop a threshold [11]. However, a comprehensive field study is required along with numerical analysis to assess the hydraulic properties, the process of rainwater infiltration, and the behavior of rainfall-induced slope failures. Therefore, in this study, numerical analysis was conducted along with field monitoring data to observe the influence of the hydraulic properties of the soil on slope stability. In this study, the transient flow analyses were accomplished by using SEEP/W followed by the slope stability analyses using SLOPE/W.

## 2 Site Investigation

### 2.1 Location

In this study, a field section located in Midlothian, Texas was selected (US-287). The selected 79.2 m (260 ft) long highway section was constructed over an embankment slope of 3H: 1V. The slope section underwent repetitive failures during its construction as shown in Fig. 1. The shoulder portion experienced numerous severe longitudinal edge cracks due to the downward slope movement or edge drop. After each failure incident, the slope was repaired.

**Fig. 1.** Site condition after failure in 2019.

### 2.2 Site soil properties

An extensive site investigation program was carried out using soil boring and electrical resistivity imaging. Based on the investigation, two distinct soil strata were identified: (1) a layer containing high-plasticity clayey soil and (2) shale. Based on the SPT-N value, the first layer is further divided into two layers of different stiffness; soft clay (0 to 3m) and medium-stiff clay (3 to 6.7m) soil. The physical characterization of the soil in the laboratory revealed the soil's high shrinkage-swelling potential. Due to the cyclic shrinkage-swelling behavior, the shear strength of this soil decreased to fully soften strength [12].

Soil's physical, strength, and hydraulic properties were determined in the laboratory. For the laboratory testing, disturbed and undisturbed samples were collected at different depths from the two boreholes and the average values were considered in the analyses. For slope soil, the moisture content varied from 10% to 40%. The liquid limit and plastic index values ranged between 55 to 74% and from 39 to 43, respectively. The clay fraction of the collected sample ranged from 85 to 95 %.

### 2.3 Field Instrumentation & Data Analysis

The test section was instrumented with the water potential and soil moisture sensors at 0.61m (2 ft), 2.1m (7 ft), and 3.1m (10 ft) depth (Fig. 2). In this study, TEROS 12 sensors (METER Group) were used to measure volumetric water content, and TEROS 21 (Fig. 3) Soil Water Potential sensors were used to measure the soil matric suction. For receiving and storing the field data, ZL6 model data loggers were used. The measurement interval was set to 60 minutes, which allowed for storing 24 data per day.

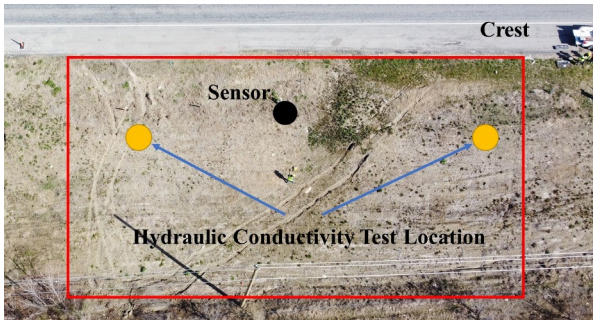


**Fig. 2.** 46m long site and the sensor and test location


**Fig. 3.** Soil moisture sensor and data logger

Fig. 4 shows the moisture sensor data of the slope. The initial moisture content values at 0.61m (2 ft), 2.1m (7 ft), and 3.1m (10 ft) depths were recorded at 44.4%, 52.1%, and 46.8%, respectively, which indicates that at the time of instrumentation, the soil's degree of saturation was similar. After initial adjustment, each sensor started showing different trends. The sensor at shallow depth (0.61m) fluctuated the most compared to the other two depths which had a noticeable coefficient of variation of 6.2%, whereas, the sensors at deeper depth (2.1m and 3.1m) had coefficients of variation of 1.27% and 1.0%, respectively. At shallow depths, the volumetric water content decreased after a series of dry days and increases suddenly after a series of rainfall.

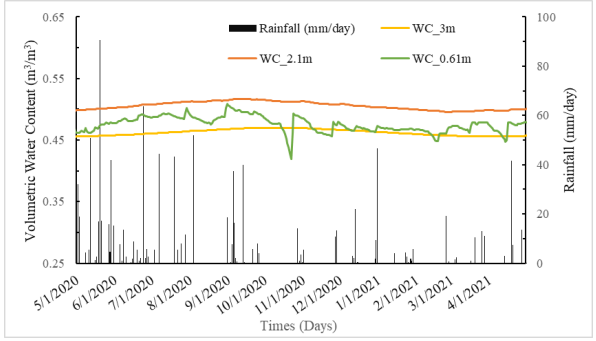


**Fig. 4.** Change in Volumetric water content at different depths

## 2.4 Field Experimental Program

Seasonal variation of the in situ hydraulic properties for the slope was monitored monthly using the Guelph permeameter (location as shown in Fig. 2). A typical Guelph Permeameter setup is presented in Fig. 5. This instrument takes the advantage of Marriotte's principle of constant head to obtain saturated hydraulic conductivity measurements and relies on the assumption that the soil in the saturation zone is isotropic, soaked uniformly, and boundaries are at infinity. Before conducting the field tests, all the components were assembled, and the reservoir was filled with water and sealed with a fill plug. Afterward, a borehole was prepared using a soil auger and the permeameter was placed in it. During the test, water was allowed to permeate the soil and the level of water in the reservoir was monitored every five-minute interval. The ratio of head loss with time was observed concurrently to detect the steady state condition of water flows through the underlying soil. For every month, two specific points were selected to take reading and the average was determined to get the field hydraulic conductivity.

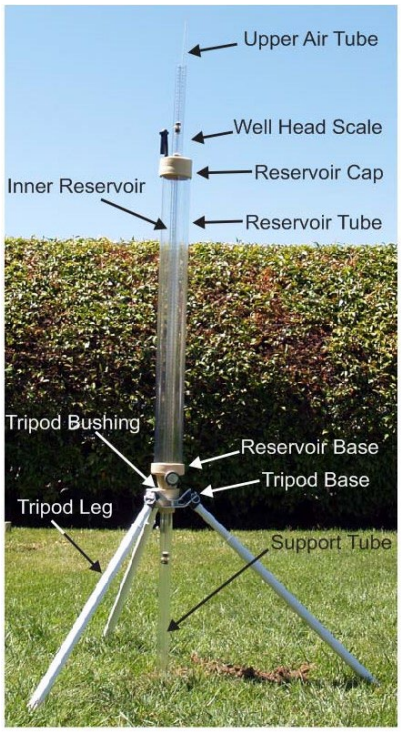


**Fig. 5.** Hydraulic conductivity test instrumentation

The field hydraulic conductivity results were monitored and analyzed using a series of equations for one head inner reservoir (equations 1 to 3). The calculated hydraulic conductivities are presented in Fig. 6 with respect to rainfall. It was observed that the hydraulic conductivity is relatively low during summer and almost 2 times higher in fall and spring. During summer, the soil is relatively dry and it forms air pockets evaporating the moisture from the soil pores. The entrapped air does not allow water to flow easily through the soil pores, resulting in less hydraulic conductivity. On the contrary, during fall and early spring, the soil pores contain varying degrees of moisture and the water can flow through them due to the capillary movement which is evident in April. In April, $4.4\times10^{-6}$ cm/s hydraulic conductivity was estimated. However, the opposite pattern was observed in late fall and early spring which indicates the saturated conditions of the soil for which the water cannot flow easily.

$$Q_1 = \bar{R}_1 \times 2.16 \quad (1)$$

$$C_1 = \left[\frac{H_2/a}{2.081 + 0.0121(H_2/a)}\right]^{0.672} \quad (2)$$

$$K_{fs} = \frac{C_1 \times Q_1}{2\pi H_1^2 + \pi a^2 C_1 + 2\pi \left(\frac{H_1}{a^*}\right)} \quad (3)$$

Where, $K_{fs}$ is soil saturated hydraulic conductivity (cm/s); C is dimensionless shape factor; R is steady state rate of fall of water in reservoir (cm/s); H is steady depth of water in boring; $a$ is the radius of well; $H_1$ is the first head of water established in borehole (cm); $H_2$ is the second head of water established in borehole (cm); $a^*$ is the microscopic capillary length parameter: 0.01 for compacted structureless clayey materials, 0.04 for fine-grained unstructured clay, 0.12 structure soil and unstructured medium to fine sand, 0.36 for coarse-grained sand and gravel, highly structured soil with large cracks.

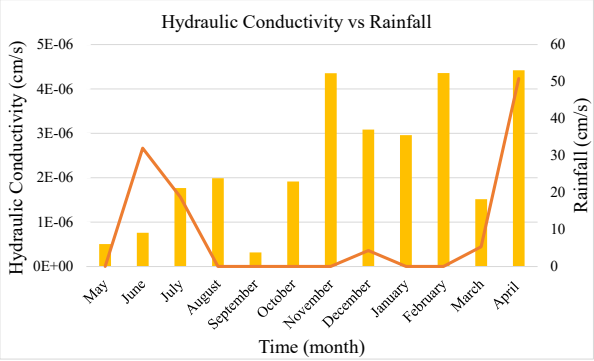


**Fig. 6.** Change in hydraulic conductivity with time.

## 3 Numerical Evaluation

The volumetric water content data obtained from the moisture sensors, the field hydraulic conductivity test results, the rainfall data, and the strength parameters obtained from laboratory test were used to numerically evaluate the slope stability. GeoStudio is a powerful finite element software that is used in this study. The SEEP/W and SLOPE/W modules were used to investigate the rainfall infiltration inside the soil and the changes in the factor of safety of the slope. A model was developed with relevant boundary conditions.

To begin with the modeling, first, a 2D model was developed using the boundary conditions as shown in Fig. 7. Three layers of the soil profile were considered where both sides had no flow condition, and the surface of the top layer was assigned rainfall intensity. Rainfall data were obtained from National Oceanic and Atmospheric Administration (NOAA) website. Then the model was calibrated with the field data. For modeling, 30% of the total rainfall was considered as 70% of the precipitation is considered as surface runoff [13].

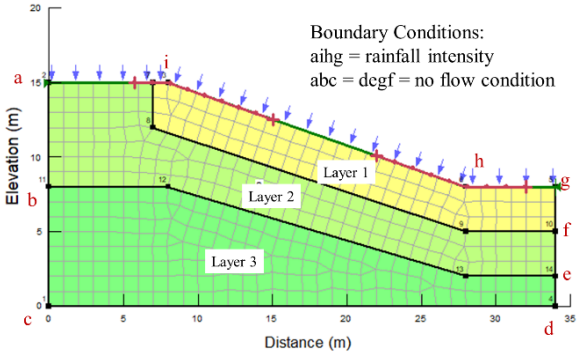


**Fig. 7.** Numerical model developed using GeoStudio.

Using the SEEP/W module in GeoStudio, seepage analysis was performed. For three different layers, the considered volumetric water content functions are shown in Fig. 8. Using this volumetric water content function, the calibration was executed to compare the actual condition in the field with the current numerical analysis. The rainfall data and the volumetric water content from the sensors of January 2020 were calibrated and compared with the current seepage analysis. From Fig. 9, it was observed that the field data and the SEEP/W analysis data show a similar pattern. However, the differences in magnitudes in the field curve and the numerical curve are evident. This is due to crack propagation and evapotranspiration occurring in the field, which was not incorporated in numerical analyses. Nevertheless, the similarity in the pattern fulfills the requirement to simulate the field conditions.

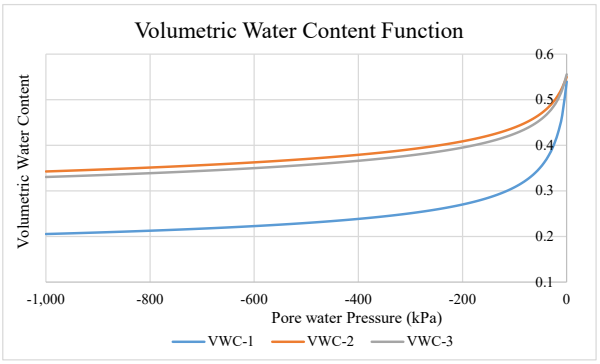


**Fig. 8.** Volumetric water content function for three layers.

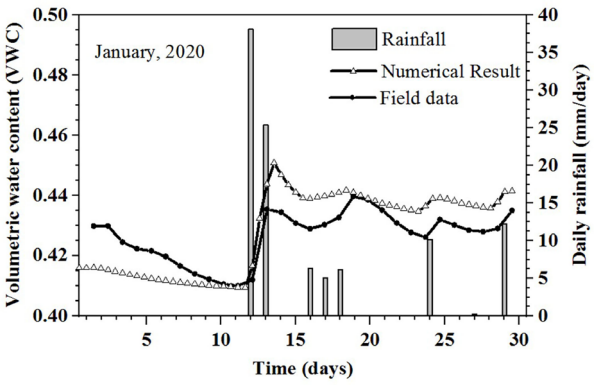


**Fig. 9.** Calibration of field data with numerical analysis.

After the calibration of the model, the hydraulic conductivity was changed monthly according to the

field data shown in Fig. 6. In the SLOPE/W analysis, the strength properties that were considered in this current study are shown in Table 1. These values were obtained from the laboratory tests that were performed on the undisturbed soil collected from the site. Throughout the numerical modeling, the strength properties were kept constant to observe the change in the factors of safety due to the change in hydraulic conductivity only.

**Table 1.** Strength properties used in numerical analysis (obtained from lab test data)

| Layer | Unit Weight (kN/m$^3$) | Cohesion (kPa) | Friction Angle (°) | Phi-B (°) |
|---|---|---|---|---|
| 1 | 17.28 | 5.31 | 11.6 | 5.8 |
| 2 | 18.07 | 1.63 | 21.06 | 10.53 |
| 3 | 20.05 | 214.3 | 0 | 0 |

## 3.1 Numerical Data Analysis

The output from SEEP/W and SLOPE/W analysis is presented in this section. Both analyses were performed for the data obtained from May 2020 to April 2021 to include one full cycle of the monitoring results.

### *3.1.1 Pore Water Pressure*

The figures (Fig. 10) below represent the porewater pressure diagram at the end of each month. From Fig. 10 (a) to Fig. 10 (d), the seepage of water is shown over a period of one year. The porewater pressure profiles for 4 months are presented in the figures. The blue line in each figure represents the zero pressure line. Since the hydraulic conductivity becomes almost twice in the 3rd and 4th months as compared to the initial, the percolation of water is well observed in Fig. 4.

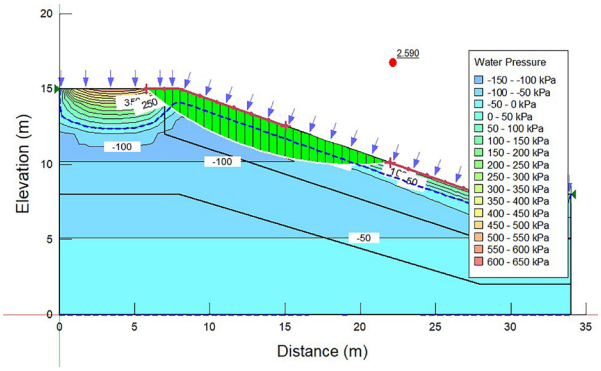


**Fig. 10 (a).** Porewater pressure diagram in May 2020.

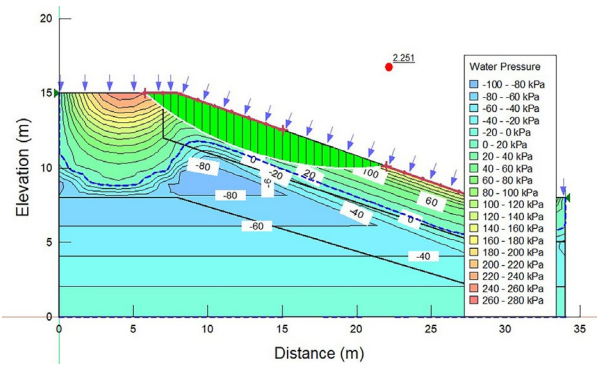


**Fig. 10 (b).** Porewater pressure diagram in September 2020.

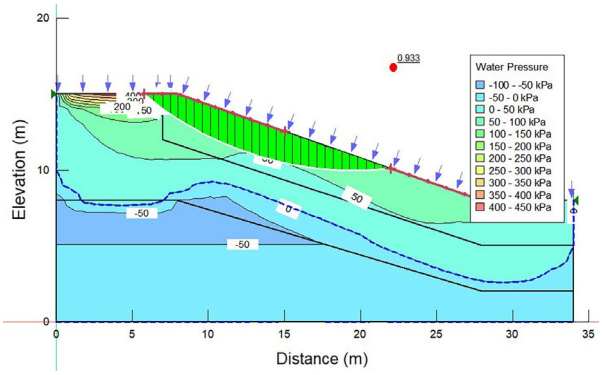


**Fig. 10 (c).** Porewater pressure diagram in December 2020.

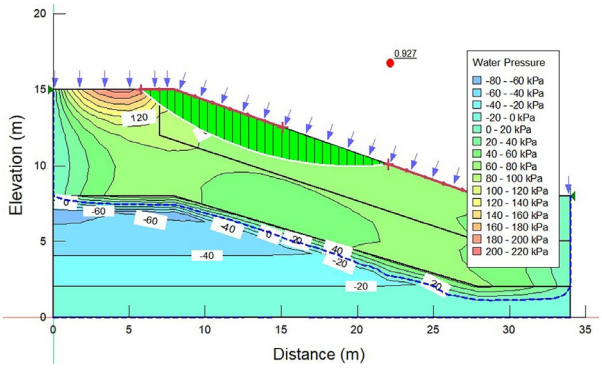


**Fig. 10 (d).** Porewater pressure diagram in April 2021.

It can also be observed that the zero pressure line goes down gradually as water seeps slowly through the pore in the soil from May 2020 to November 2020. In December the drop is very significant. At the red-marked point, the porewater pressure increases from 20 kPa to 50 kPa which is an increment of almost 200%. From May 2020 to November 2020, this rate of increase was less than 70%. Later the hydraulic conductivity was estimated to be high, therefore, the porewater pressure was more than 20 kPa all across the slope section.

The hydraulic conductivity of the 2nd and the 3rd layer was considered $10^{-6}$ and $10^{-10}$ cm/s, respectively. Due to very low hydraulic conductivity, there was no appreciable seepage in 3rd soil layer.

### *3.1.2 Factors of Safety*

The major objective of this study was to determine the factor of safety of the slope and understand the rationalization of repetitive failure. From Fig. 11, the pattern of a slope failure (in terms of the factor of safety) can be explained.

For the initial 60 days, it was observed that the factor of safety increases almost 175% from 2 to 3.5. Initially, the water took time to seep through the pores since the hydraulic conductivity was very low in May and June 2020. However sudden drop was observed after a high-intensity rainfall. After 60 days, relatively higher hydraulic conductivity was estimated which was greater than the initial condition, The water started seeping through the soil easily compared to the previous condition, and accordingly, the drop in factor of safety was observed from day 60 to day 120. The factor of

safety decreased nearly 3 times during this period from 3.5 to 1.3.

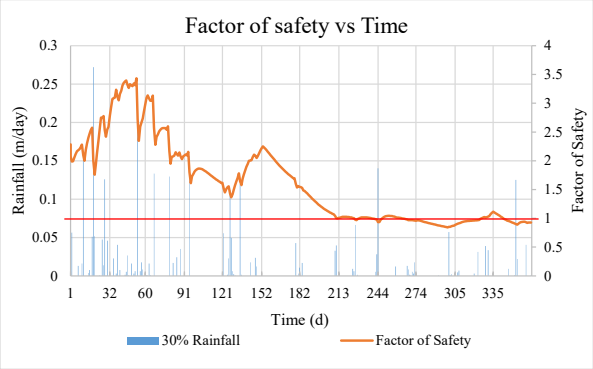


**Fig. 11.** Change in factor of safety with time.

From day 120 to day 150 (September 2020) the hydraulic conductivity was very low and the amount of rainfall was not signifiant as in the other months, the factor of safety tends to increase. However, after September 2020, the hydraulic conductivity started to incease to $4\times10^{-6}$ cm/s and water started seeping into the slope easily and generating high porewater pressure which eventually decreased the shear strength of the soil. Therefore, the factor of safety dropped below one, which indicates the failure of the slope. Furthermore, the depth of the critical failure surface was observed at 1.5-2m as shown in Fig. 10(c).

## 4 Conclusion

In this current study, a location along the highway was selected that underwent several repetitive slope failures and the reason behind this was investigated. Volumetric water content and in-situ hydraulic conductivity were monitored using moisture sensors and a Guelph permeameter. These data along with the lab test results were used to numerically replicate the field condition using the finite element software GeoStudio. The study concludes the following:

1. The rainfall intensity plays a significant role in the changes in hydraulic conductivity and volumetric water content.
2. The change in volumetric water content was prominent at 1 m. At 2 m and 3 m depth, the volumetric water content was the same throughout the monitoring period.
3. Hydraulic conductivity greater than $4\times10^{-6}$ cm/s and high volumetric water content generated higher porewater pressure which eventually leads to slope failure.
4. The failure occurred at the shallow depth as found from the different slip circles in the numerical analysis. The failure depth was almost 1.5-2 m.

## References

1. S. G. Wright, *Evaluation of Soil Shear Strengths for Slope and Retaining Wall Stability Analyses with Emphasis on High Plasticity Clays*, FHWA/TX-06/5-1874-01-1, Federal Highway Administration, Washington, D.C, (2005).
2. S. J. Abbey, E. U. Eyo, & S. Ng'ambi. Bull. Eng. Geol. Environ. **79**, 2119 (2020)
3. W. Mccormick, and R. Short, *Cost Effective Stabilization of Clay Slopes and Failures using Plate Piles*, in Proceedings of the IAEG2006, The Geological Society of London, London, United Kingdom, 1-7, (2006).
4. C. S. Tang, X. J. Pei, D. Y. Wang, B. Shi, & J. Li, J. Geotech. Geoenv. Eng. **141(4)**, 04014122. (2015)
5. J. Hossain, *Geohazard potential of rainfall-induced slope failure on expansive clay*. Doctoral dissertation, The University of Texas at Arlington, Arlington, Texas, USA, (2013)
6. S. Wang, G. Idinger, & W. Wu, Acta Geotech. **16(9),** 2899 (2021)
7. E. Damiano, & L. Olivares. Nat. Hazards, **52(2)**, 329 (2010)
8. M. A. Islam, M. S. Islam, & T. E. Elahi, *Effectiveness of vetiver grass on stabilizing hill slopes: a numerical approach.* In Proceedings of the Geo-Congress 2020: Engineering, Monitoring, and Management of Geotechnical Infrastructure, Reston, VA, USA: American Society of Civil Engineers, 106 (2020)
9. H. Rahardjo, T. H. Ong, R. B. Rezaur, & E. C. Leong. J. Geotech. Eng. **133**, 1532 (2007)
10. M.A. Islam, A. A. Jeet, N. Gupta, A. Gupta, & T. Islam, *Factors Affecting the Stability and Behavior of an MSE Wall: A Numerical Approach*, In Proceedings of the Geo-Congress 2022, 375-385 (2022)
11. M. A. Islam, *Rainfall-Induced Slope Failure – An Early Warning System*, Doctoral Dissertation, The University of Texas at Arlington, Arlington, Texas, USA, (2021)
12. A. Saleh, and S.G. Wright, *Shear strength correlations and remedial measure guidelines for the long-term stability of slopes constructed of highly plastic clay soils*, No. FHWA/TX-98/1435-2F, Federal Highway Administration, Washington, D.C, (2017)
13. G. H. Yunusa, & N. Gofar. Int. J. Phys. Sci. **7(3)**, 508 (2012).